



Vapor growth of V-doped MoS₂ monolayers with enhanced B-exciton emission and broad spectral response

Biyuan Zheng¹ · Xingxia Sun¹ · Weihao Zheng² · Chenguang Zhu¹ · Chao Ma¹ · Anlian Pan¹ · Dong Li¹ · Shengman Li^{1,3}

Received: 15 September 2023 / Accepted: 3 November 2023
© The Author(s) 2023

Abstract

Dynamically engineering the optical and electrical properties in two-dimensional (2D) materials is of great significance for designing the related functions and applications. The introduction of foreign-atoms has previously been proven to be a feasible way to tune the band structure and related properties of 3D materials; however, this approach still remains to be explored in 2D materials. Here, we systematically demonstrate the growth of vanadium-doped molybdenum disulfide (V-doped MoS₂) monolayers via an alkali metal-assisted chemical vapor deposition method. Scanning transmission electron microscopy demonstrated that V atoms substituted the Mo atoms and became uniformly distributed in the MoS₂ monolayers. This was also confirmed by Raman and X-ray photoelectron spectroscopy. Power-dependent photoluminescence spectra clearly revealed the enhanced B-exciton emission characteristics in the V-doped MoS₂ monolayers (with low doping concentration). Most importantly, through temperature-dependent study, we observed efficient valley scattering of the B-exciton, greatly enhancing its emission intensity. Carrier transport experiments indicated that typical p-type conduction gradually arisen and was enhanced with increasing V composition in the V-doped MoS₂, where a clear n-type behavior transited first to ambipolar and then to lightly p-type charge carrier transport. In addition, visible to infrared wide-band photodetectors based on V-doped MoS₂ monolayers (with low doping concentration) were demonstrated. The V-doped MoS₂ monolayers with distinct B-exciton emission, enhanced p-type conduction and broad spectral response can provide new platforms for probing new physics and offer novel materials for optoelectronic applications.

Keywords Atomic substitution · V-doped MoS₂ · Distinct B-exciton · Broad spectral response

1 Introduction

Two-dimensional (2D) semiconductors have attracted attention due to their future application in field effect transistors [1–6], photodetectors [7–10], laser [11, 12], photoelectrochemical [13], and other devices [14, 15]. Molybdenum disulfide (MoS₂), as a typical 2D semiconductor, has direct band gap (~1.8 eV) [16–18] and high mobility [1, 5], and shows great potential in optoelectronic devices [1–3, 5, 8, 14]. Due to the broken inversion symmetry, inducing the spin–orbit coupling, there is a large splitting of ~160 meV over the valence band in monolayer MoS₂, giving rise to A- and B-excitons [16, 18–20]. Generally, A-exciton behavior dominates the emission of the MoS₂, while observing B-exciton behavior is difficult due to the forbiddance of its transition [17, 21]. Meanwhile, achieving p-type conductivity in chemical vapor deposition (CVD) grown MoS₂ monolayer is challenging because of its insurmountable sulfur

✉ Dong Li
liidong@hnu.edu.cn

✉ Shengman Li
smli@hnu.edu.cn

¹ Key Laboratory for Micro-Nano Physics and Technology of Hunan Province, State Key Laboratory of Chemo/Biosensing and Chemometrics, Hunan Institute of Optoelectronic Integration, College of Materials Science and Engineering, Hunan University, Changsha 410082, China

² College of Advanced Interdisciplinary Studies and Hunan Provincial Key Laboratory of Novel Nano Optoelectronic Information Materials and Devices, National University of Defense Technology, Changsha 410073, China

³ Wuhan National Laboratory for Optoelectronics (WNLO), Huazhong University of Science and Technology (HUST), Wuhan 430074, China

vacancy defect [22, 23]. Furthermore, due to the large band gap, photodetectors based on MoS₂ monolayers show a limited detection range in visible light [8]. Consequently, effectively manipulating the photoelectric properties of MoS₂ and further enriching its properties are important for both fundamental research and applications.

Foreign substitutional doping is efficacious, stable, and exhibits long-range ordering, making it a preferred method for altering the electronic band structure, conduction type, and carrier concentration of pristine materials. Previous reports suggested that vanadium (element V) is an attractive dopant for room-temperature ferromagnetism and has found widespread use in many magneto-optic devices [24–27]. The introduction of V element in MoS₂ offers an effective means to modulate both the optical and the electrical properties of the samples, potentially leading to new applications and functionalities. Very recently, CVD growth of V-doped MoS₂ for use in synaptic transistors and quasi-continuously tunable carrier polarity transistors have been reported [28–30]. However, to the best of our knowledge, the A- and B-excitons properties and the photoelectric applications of V-doped MoS₂ have not been systematically studied.

In this work, V-doped MoS₂ monolayers were grown using an alkali metal-assisted CVD approach. The achievement of V doping in high-quality crystalline monolayers were confirmed by scanning transmission electron microscopy (STEM), X-ray photoelectron spectroscopy (XPS) and Raman spectra. The emergence of p-type conduction in the achieved samples further demonstrated the successful introduction of V atoms into the crystal structure. What's even more interesting is, the distinct B-exciton emission, enhanced p-type conduction and broad spectral response observed in the V-doped MoS₂. Our results could offer a novel approach to modulating exciton properties in 2D semiconductors and potentially trigger numerous applications in spintronics.

2 Experimental

2.1 Materials synthesis

A one-zone furnace was used for growth of V-doped MoS₂ monolayers. Firstly, one quartz boat (boat 1), loaded with sublimate sulfur powder (S), was placed at the upstream, while another (boat 2), containing a mixture of molybdenum trioxide (MoO₃, Alfa Aesar, 99%), vanadium pentoxide (V₂O₅, Alfa Aesar, 99%), and potassium iodide (KI, Alfa Aesar, 99%), was positioned at the center of a quartz tube (25 cm in diameter and 100 cm long). A long piece of SiO₂/Si (270 nm SiO₂, 1 cm × 3 cm) substrate was placed above the quartz boat 2. The quartz tube containing the reaction sources and the deposited substrate was placed in the

furnace, and the quartz boat 2 was ensured to be located in the center of the furnace. High purity Ar was introduced from the upstream as carrier gas and discharged from the downstream of the quartz tube. Prior to heating, high-rate Ar gas flow (1000 SCCM) was used to remove any active gases. The furnace was then heated to 750–800 °C in 30 min and held at that temperature for 5–10 min to grow the V-doped MoS₂ monolayers. Throughout the growth process, the Ar gas flow was maintained at 50 SCCM. Subsequent to growth, the furnace was then allowed to cool naturally to room temperature.

2.2 Characterizations

Raman and photoluminescence (PL). The Raman/PL was performed using a μ -PL system (WITec, alpha-300) equipped with a 532 nm argon ion laser.

Atomic force microscope (AFM). The AFM observations were carried out using a Bruker Dimension ICON instrument.

Scanning transmission electron microscopy. The STEM observations were acquired using a JEOL ARM200F microscope.

2.3 Device fabrication and measurements

Source-drain electrodes of the back-gated V-doped MoS₂ devices were fabricated using a transfer method. Au with a thickness of 50 nm was prepared on a bare SiO₂/Si substrate using photolithography and thermal evaporation deposition methods and subsequently transferred onto the top of the V-doped MoS₂ monolayers as source/drain. The optoelectrical properties of the V-doped MoS₂ devices were measured using Lake Shore Probe Station and Agilent B1500A semiconductor analyzer.

3 Results and discussion

V-doped MoS₂ monolayers were synthesized using an alkali metal-assisted CVD method as depicted in Fig. 1a. As is the case in previous reports, the chemical reaction between MoO₃, V₂O₅ and the KI results in formation of volatile oxyhalide species [31, 32]. In brief, solid-phase MoO₃ reacts with solid-phase KI, producing the gaseous-species MoO₂I₂. Similarly, the solid-phases V₂O₅ and KI react with each other to form gaseous-phase VOI₃. The gas–gas phase reactions among MoO₂I₂, VOI₃ and S could occur easily and efficiently. The possible reaction routes in the system are listed as follows:



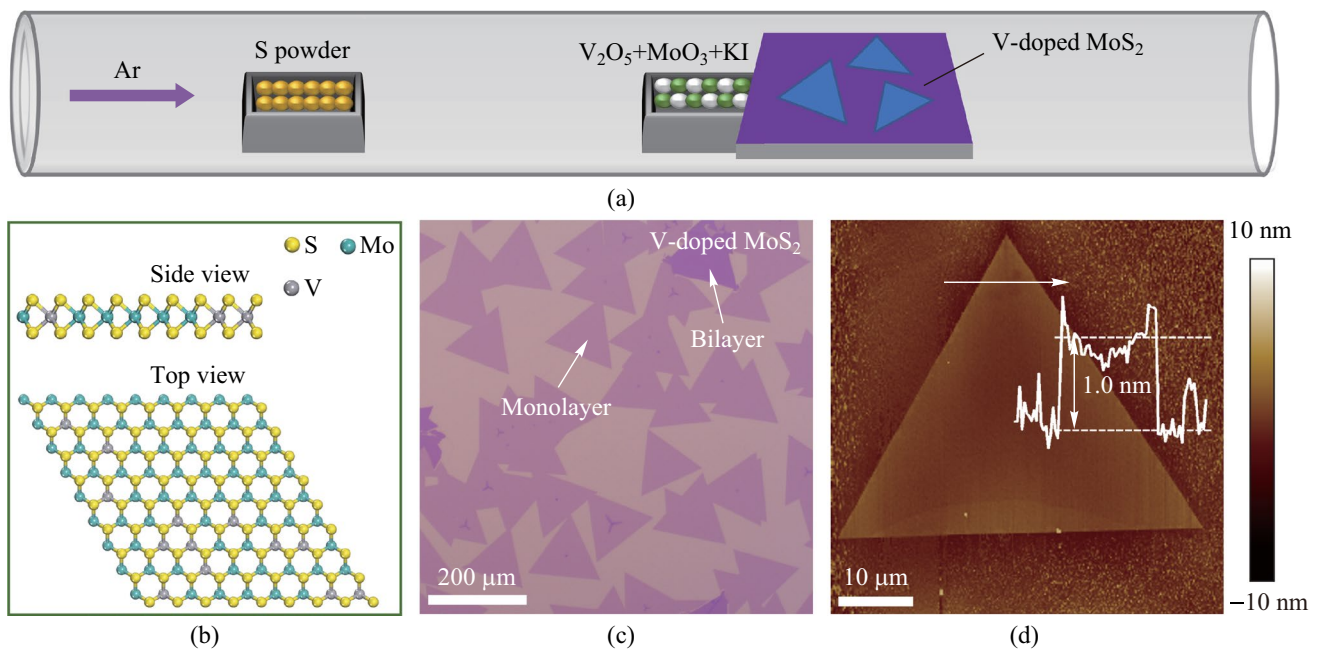


Fig. 1 Schematic of vapor growth and AFM characterization of V-doped MoS₂ monolayers. **a** Schematic of the synthesis process of V-doped MoS₂ monolayers. **b** Side- and top-views of the crystal structure of V-doped MoS₂ monolayer. The yellow, blue and gray spheroids represent S, Mo and V atoms, respectively. **c** Optical image of the V-doped MoS₂ monolayers. **d** AFM image of the V-doped MoS₂ monolayer. Inset: height profile of the V-doped MoS₂ measured along white arrow in **(d)**, indicating that the thickness of detected sample is about 1.0 nm

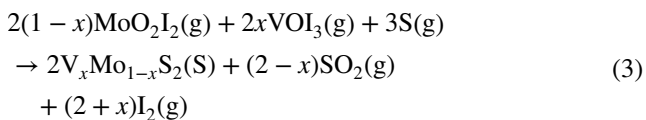
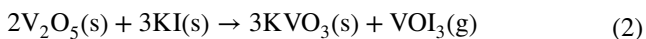


Figure 1b displays the side- and top-views of the atomic structure of the V-doped MoS₂ monolayer, wherein the yellow, blue and gray spheroids represent the S, Mo and V atoms, respectively. V atoms have substituted and occupied the sites of Mo atoms. Figure 1c shows the optical image of the V-doped MoS₂ monolayers, indicating the uniform distribution on a large scale (> 100 μm). Additionally, though in a small proportion, V-doped MoS₂ bilayers with deeper contrast than monolayers were observed and are marked in Fig. 1c. AFM characterization was used to confirm the thickness of the V-doped MoS₂ nanosheet (Fig. 1d), which was measured to be about 1.0 nm (inset in Fig. 1d), indicating a single layer nature.

The atomic structure and chemical composition of the V-doped MoS₂ monolayers were investigated by STEM, energy dispersive X-ray spectroscopy (EDS), high-resolution STEM (HRSTEM) and selected-area electron diffraction (SAED). Figure 2a displays a typical low-magnification annular dark-field (ADF) STEM image of

a single-domain V-doped MoS₂ sample transferred onto a Cu grid. In Fig. 2b, the EDS spectrum obtained from the white dot in Fig. 2a revealed elemental peaks corresponding to S, Mo, and V, confirming the composition of the doped nanosheets. Thus, we could deduce the V mole fraction of the V-doped MoS₂ sample, indicating a composition of V_{0.11}Mo_{0.89}S₂. Figure S1 shows the EDS spectra taken from more samples, these samples were used for Raman, PL and electrical characterizations.

Figure 2c presents the SAED pattern of the sample, displaying a single set of diffraction spots with sixfold symmetry, confirming the single-crystal nature of V-doped MoS₂. The lattice spacing of the V-doped MoS₂ was obtained using the diffraction peaks yields (100) and was measured to be 0.272 nm, which is similar with that of MoS₂ [5]. HRSTEM was employed to characterize the atomic structure of the achieved V-doped MoS₂ (Fig. 2d), in which the different atoms could be identified using Z-contrast ($Z^2_{\text{Mo}} = 1764$, $Z^2_{\text{V}} = 529$ and $Z^2_{\text{S}} + Z^2_{\text{S}} = 512$). Figure 2e and f provide enlarged experimental and simulation HRSTEM images, in which V atoms are marked with yellow dotted circles. As shown in Fig. 2g, the ADF intensity profile acquired along the blue arrow in Fig. 2e and f also confirms similar results.

XPS was adopted to characterize the chemical states of elements in another V-doped MoS₂ sample. From the XPS survey spectra as shown in Fig. S2, we determined that the

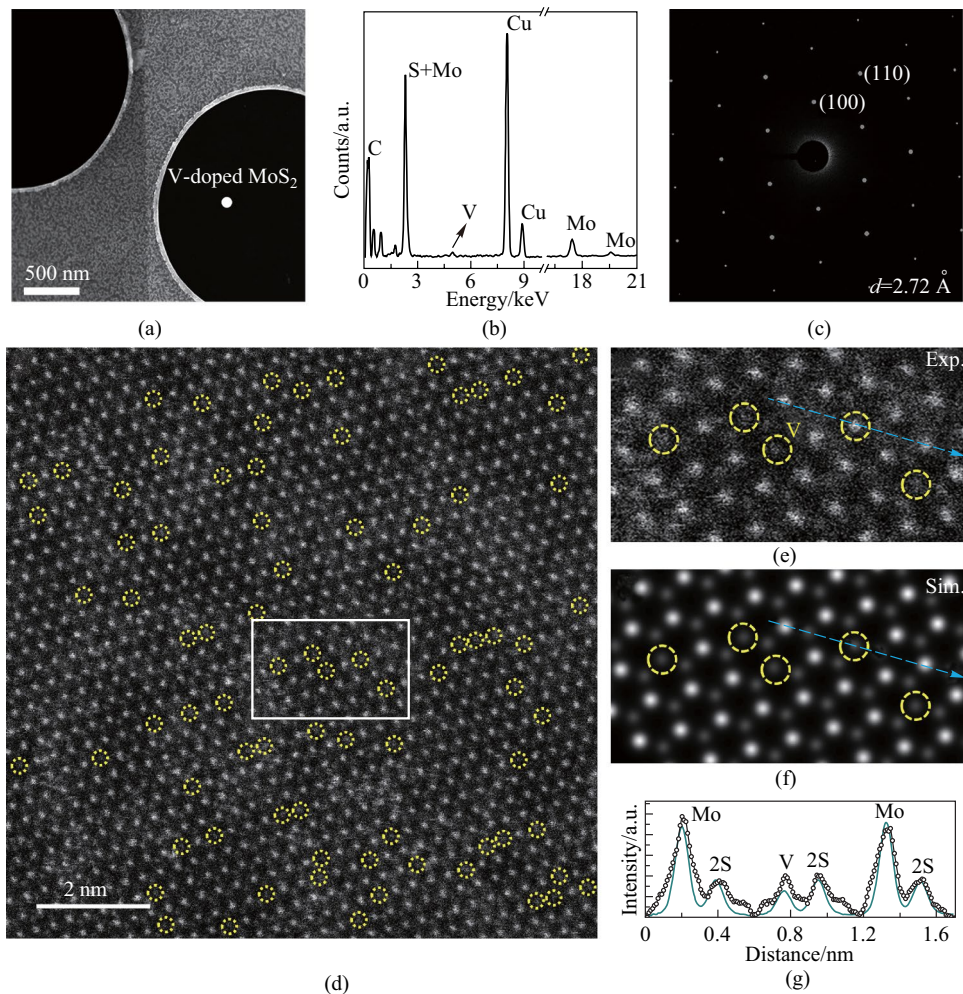
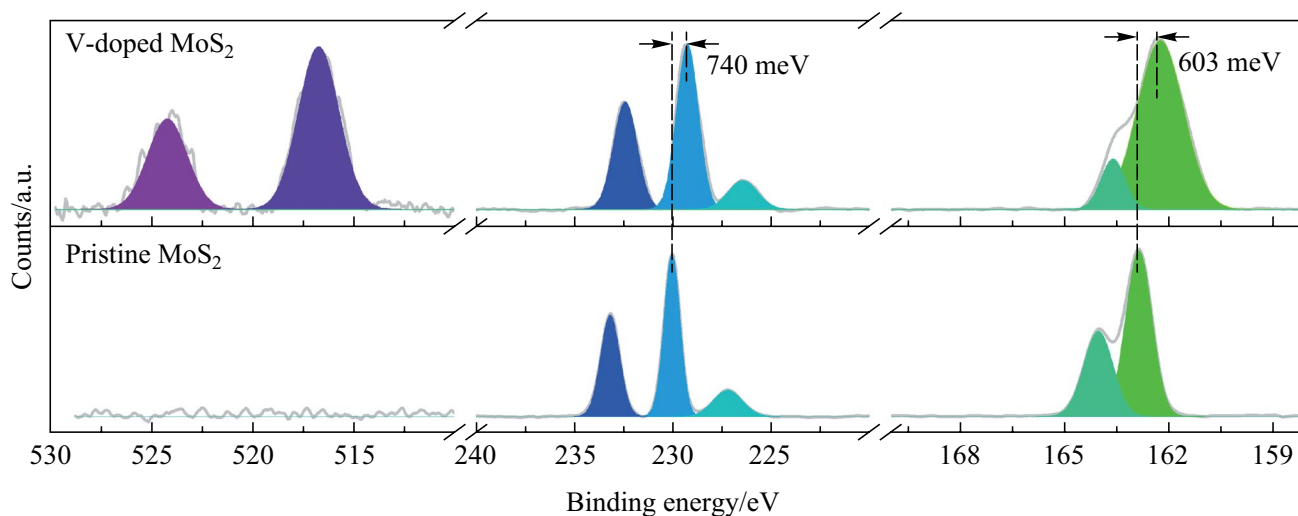


Fig. 2 Structural and chemical composition of V-doped MoS₂ monolayer. **a** Low-magnification ADF STEM image of the V-doped MoS₂ monolayer. **b** TEM–EDX profile collected from white dot in **(a)**, shows the V mole fraction (x) is 0.11. **c** SAED pattern of the V-doped MoS₂ monolayer along the zone axis of [0001]. **d** HRSTEM image of the V-doped MoS₂ monolayer, the V atoms are highlighted by yellow dotted circles. **e, f** Enlarged, **e** experimental, and **f** simulation HRSTEM images of the yellow rectangle region in **(d)**. **g** Electron intensity profile along the blue arrows in **(e)** and **(f)**

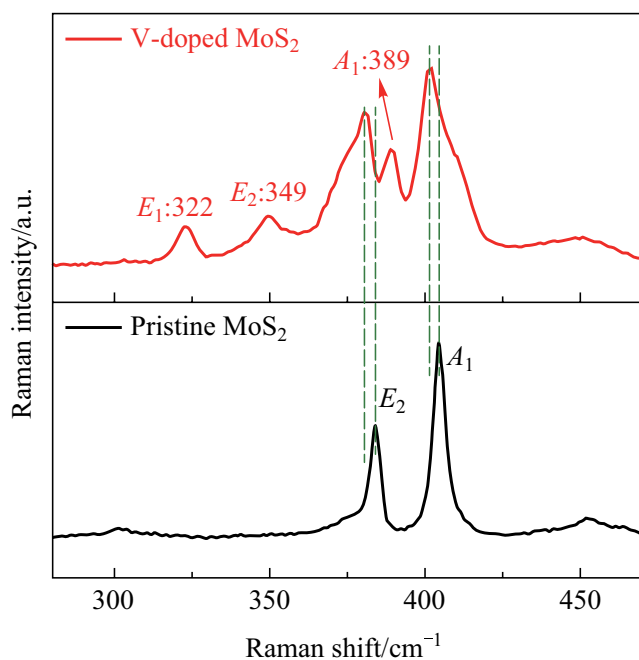
V mole fraction (x) of the tested samples was 9%, indicating a composition of V_{0.09}Mo_{0.91}S₂. Figure 3a shows the element binding energy comparison between V-doped MoS₂ (upper half) and pristine MoS₂ (lower half). For MoS₂, five peaks were observed at 233.2, 230.0, 227.2, 164.0 and 162.9 eV. The first two peaks are attributed to the Mo element (Mo⁴⁺ 3d_{3/2} and Mo⁴⁺ 3d_{5/2}), while the remaining peaks belong to S element (S²⁻ 2s, S²⁻ 2p_{3/2} and S²⁻ 2p_{1/2}) [33]. In the case of V-doped MoS₂, a slight down-shift of the above peaks was observed. Such down-shift indicated that the Fermi level of the achieved V-doped MoS₂ was closer to the valence band compared with that of the pristine MoS₂ monolayer, which demonstrated an increase in p-type doping concentration [34, 35]. Moreover, two additional peaks located at 516.7 and 524.3 eV were observed, which was attributed to the

presence of V atoms. These two peaks were indexed as V⁴⁺ 2p_{3/2} (516.7 eV) and V⁴⁺ 2p_{1/2} (524.3 eV) [36].

Raman spectra were used to investigate the vibration modes of the V-doped MoS₂ monolayers (V_{0.11}Mo_{0.89}S₂), while pristine MoS₂ was chosen as a representative sample. Pristine MoS₂ exhibited two Raman peaks centered at 384 and 404 cm⁻¹, corresponding to the E_{2g(S-Mo)} mode and the A_{1g(S-Mo)} mode, respectively (bottom panel in Fig. 3b). However, in the Raman spectrum collected from the V-doped MoS₂ monolayer (top panel in Fig. 3b), four additional peaks located at 323, 349, 389 and 406 cm⁻¹ were observed, indicating the introduction of V atoms [37, 38]. It is worth noting that, compared with pristine MoS₂, the E_{2g(S-Mo)} and A_{1g(S-Mo)} peaks taken from V-doped sample exhibited a slight down-shift of 2.82 and 2.96 cm⁻¹, respectively, further



(a)



(b)

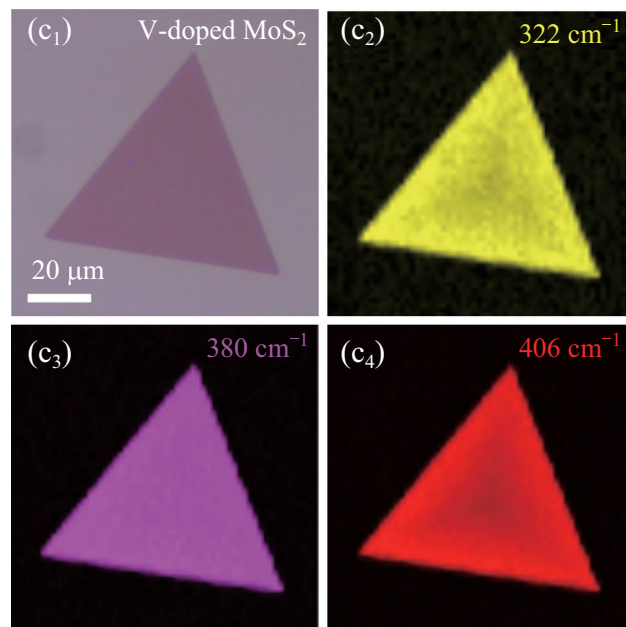


Fig. 3 XPS and Raman characterizations of V-doped MoS₂ monolayers. **a** XPS spectra of the V-doped MoS₂ (upper half) and pristine MoS₂ (lower half) monolayers, respectively. **b** Raman spectra of the V-doped MoS₂ (upper half) and pristine MoS₂ (lower half) monolayers, respectively. **c**₁ Optical and **c**₂–**c**₄ Raman intensity mapping images of the selected V-doped MoS₂ monolayer

implying hole doping induced by V atoms [34]. Raman mapping images of the V-doped MoS₂ monolayer (as shown in Fig. 3c) demonstrated the uniform chemical composition of the tested sample.

The optical properties of the V-doped MoS₂ monolayers were investigated with steady-state PL spectroscopy. Figure 4a shows the optical image of a selected V-doped MoS₂ monolayer with low doping concentration (V_{0.05}Mo_{0.95}S₂). The typical PL spectrum collected from pristine MoS₂

(depicted by a black line in Fig. 4d) exhibited two peaks centered at 1.85 and 2.00 eV, corresponding to A- and B-excitons, respectively. Clearly, the A-exciton emission dominated the whole emission behavior. The ratio of the emission integrated intensities between the B- and A-excitons was calculated as $\eta_p = I_B/I_A = 0.083$, where I_A and I_B are the integrated intensities of A- and B-excitons, respectively. In contrast, the spectrum of the V-doped MoS₂ (illustrated by a red line in Fig. 4d) showed distinct B-exciton emission

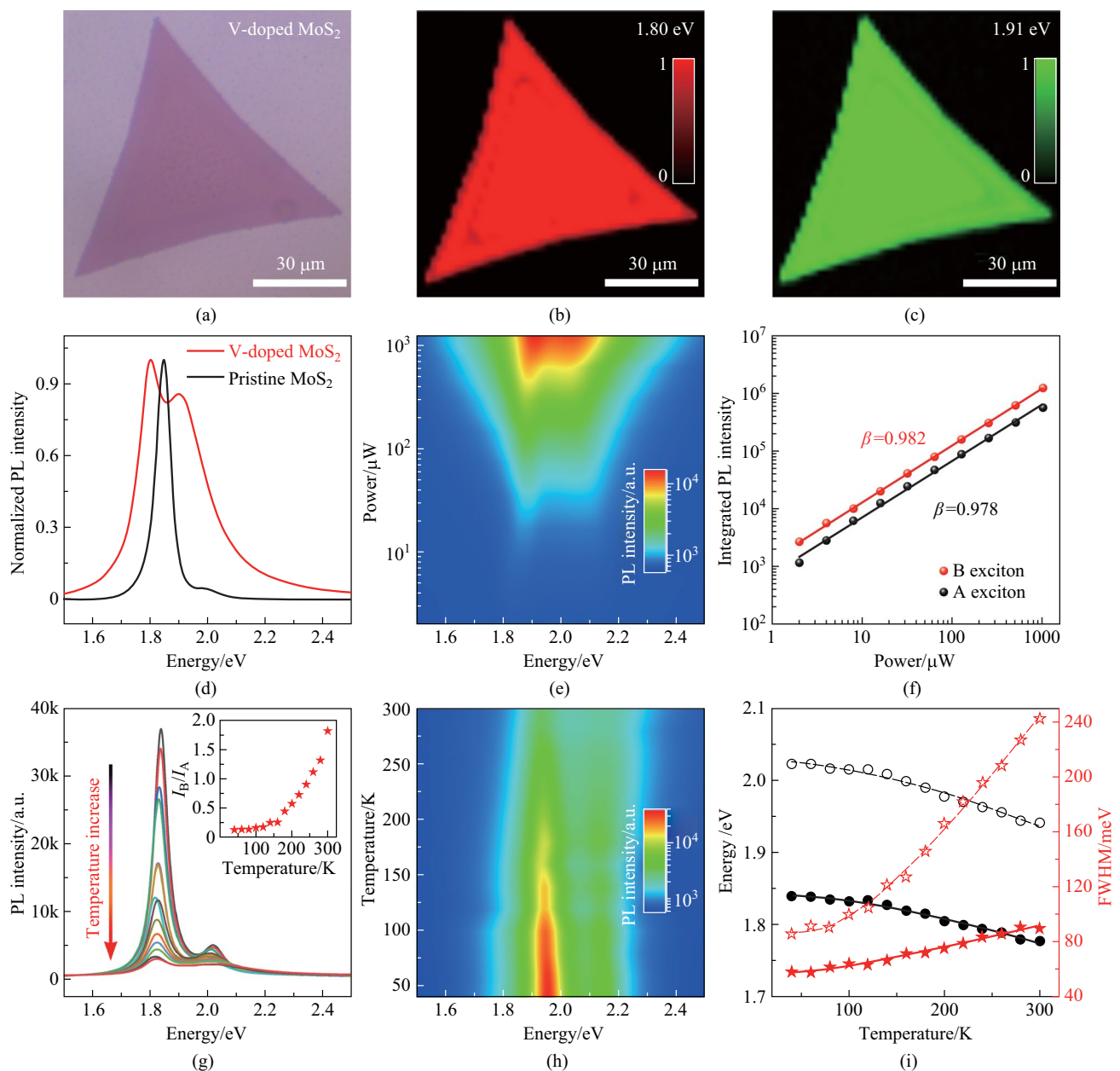


Fig. 4 Optical characterization of V-doped MoS₂ monolayers. **a** Optical image and **b**, **c** PL intensity mapping images of the V-doped MoS₂ monolayer at **b** 1.80 eV and **c** 1.91 eV, respectively. **d** Normalized PL spectra of the pristine MoS₂ (black line) and V-doped MoS₂ (red line) monolayers. **e** 2D pseudocolor plot of the emission spectra under illumination by the laser excitation power densities from 2 to 1240 μW. **f** Integrated PL intensities of the A- and B-excitons. **g** PL spectra from the V-doped MoS₂ monolayer from 40 to 300 K. Inset: presents the emission intensities ratio η_p between the A- and B-excitons at different temperatures. **h** 2D pseudocolor plots of temperature-dependent PL spectra of the V-doped MoS₂ monolayer. **i** Corresponding optical band gap and PL FWHM as a function of temperature together with their fits

that did not occur in the case of pristine MoS₂. The η_p of the V-doped MoS₂ was calculated to be 3.13, which was 38 times higher than that occurring in the case of pristine MoS₂ monolayer. In addition, noticeable red-shifts of both the emission peaks of A- (~46 meV) and B-excitons (~99 meV) were observed in the V-doped MoS₂ monolayer, primarily resulting from doping-induced bandgap narrowing [39].

The split of A- and B-exciton bands ($\Delta_{BA} = E_B - E_A$) was determined to be ~110 meV for V-doped MoS₂ monolayer, smaller than that of pristine MoS₂ monolayer of ~150 meV, indicating that the doped V atoms effectively reduced the spin-orbit splitting between A- and B-excitons behavior in MoS₂ monolayer (Fig. S3). As shown in Fig. S4, for the V_{0.02}Mo_{0.98}S₂ and V_{0.05}Mo_{0.95}S₂ monolayers (with low

doping concentration), the η_p increased with the increase of V composition. But the sample with high doping concentration ($V_{0.11}Mo_{0.89}S_2$) did not have PL emission. Such PL quenching is contributed to the localized exciton trapped states caused by doped V atoms (Fig. S3) [39].

Figure 4b and c show the energy-selected PL intensity mapping images of the V-doped MoS_2 at 1.80 and 1.91 eV, respectively. The slightly non-uniform PL mapping is mainly caused by strain effects [40]. To further explore the spectral features, we studied the excitation power dependence of A- and B-excitonic transitions. Figure 4e presents the 2D pseudocolor plots of PL spectra under illumination by different laser excitation power densities. The log–log plots of integrated PL intensities of the A- (black dots in Fig. 4f) and B-excitons (red dots in Fig. 4f), as functions of excitation power, are presented in Fig. 4f. The relationship between integrated PL intensity I and excitation power P can be written as: $I = P^\beta$, where $\beta \approx 1$ implies an exciton-like transition [41]. Temperature-dependent experiments were conducted to explore the distinct B-exciton emission. Figure 4g exhibits the PL spectra measured in the V-doped MoS_2 monolayer at different temperatures, while the corresponding 2D pseudocolor results are shown in Fig. 4h. The inset in Fig. 4g presents the integrated intensities ratio (η_p) of A- and B-excitons at different temperatures. As can be seen, η_p increased gradually with rising temperature, indicating the activation of B-exciton emission was at high temperature. This can be attributed to the enhancement of efficient valley scattering with the assistance of phonons (Fig. S3) [42]. On the contrary, the abnormal behavior here was attributed to the efficient valley scattering induced by the V atoms doping, which should be largely suppressed at low temperature, subsequently quenching the B-exciton emission.

In addition, we also studied the exciton-phonon interactions of the V-doped MoS_2 monolayer. As can be seen, the two emission peaks broadened and shifted towards lower energy with increasing the temperature (Fig. 4i). Such variation can be well interpreted in terms of by Varshni’s semi-empirical formula:

$$E_g(T) = E_g(0) - \frac{\alpha T^2}{T + \beta}, \tag{4}$$

where α and β are the characteristics of the given material. We found that the energies shift of A- and B-excitons of the V-doped MoS_2 matched well Eq. (4), and the results are

Table 1 Fitting results of PL energies shift at different temperatures

Exciton	$E_g(0)/eV$	$\alpha/(eV \cdot K^{-1})$	β/K
A-exciton	1.843 ± 0.002	$(6.258 \pm 2.595) \times 10^{-4}$	514.83 ± 341.89
B-exciton	2.027 ± 0.003	$(8.815 \pm 4.420) \times 10^{-4}$	566.25 ± 438.83

Table 2 Fitting results of PL FWHM at different temperatures

Exciton	Γ_0/meV	Γ_{LO}/meV	ω_{LO}/eV
A-exciton	57.523 ± 1.216	37.036 ± 11.762	25.616 ± 6.044
B-exciton	86.375 ± 2.108	313.684 ± 39.271	38.074 ± 2.838

shown in Table 1. Such observed unequal shifts of A- and B-excitons were quite similar to those of other TMDCs [42].

Full width variation at half-maximum (FWHM) of these spectra is shown in Fig. 4i, which can be described by Bose–Einstein type expression:

$$\Gamma(T) = \Gamma_0 + \frac{\Gamma_{LO}}{e^{\omega_{LO}/(kT)} - 1}, \tag{5}$$

where Γ_0 represents the inhomogeneous broadening term and the line width at 0 K, Γ_{LO} represents the exciton-longitudinal optical (LO) phonon coupling, and the ω_{LO} is the dominant phonon or an average phonon energy. The values of the parameters are summarized in Table 2. The temperature-dependent shifts of the energies and FWHM of the excitonic transitions are mainly due to the lattice constant variations and interactions with relevant acoustic and optical phonons [43].

To explore the electronic properties and applications of our achieved V-doped MoS_2 monolayers, we fabricated back-gated field-effect transistors. Figure 5a provides the schematic diagram of the device. Figure 5b shows the transport properties of the samples with different V composition (MoS_2 , $V_{0.02}Mo_{0.98}S_2$, $V_{0.05}Mo_{0.95}S_2$ and $V_{0.11}Mo_{0.89}S_2$). It is evident that both the MoS_2 and $V_{0.02}Mo_{0.98}S_2$ exhibited typical n-type unipolar transfer behavior. With the introduction of V atoms, transitions from n-type first to ambipolar and then to p-type conduction occurred, revealing that the V atom doped in MoS_2 monolayer could effectively implement p-type doping. Ambipolar conduction behavior was observed in $V_{0.05}Mo_{0.95}S_2$ based device, while p-type unipolar conduction behavior was obtained with further increases in the V doping concentration ($V_{0.11}Mo_{0.89}S_2$), which was consistent with the Raman and XPS results. The above results demonstrated that with the increase of V component, the V-doped MoS_2 exhibited a transition from non-degenerate (MoS_2 and low doping concentration V-doped MoS_2) to degenerate (high doping concentration V-doped MoS_2) semiconductor.

The photoelectric behavior of the V-doped MoS_2 was then examined and $V_{0.02}Mo_{0.98}S_2$ monolayer based device was selected. Figure 5c shows the output characteristic curves, exhibiting liner results. Figure S5 displays the photoconductive properties of the V-doped MoS_2 monolayer device under illumination by 450 and 633 nm lasers with

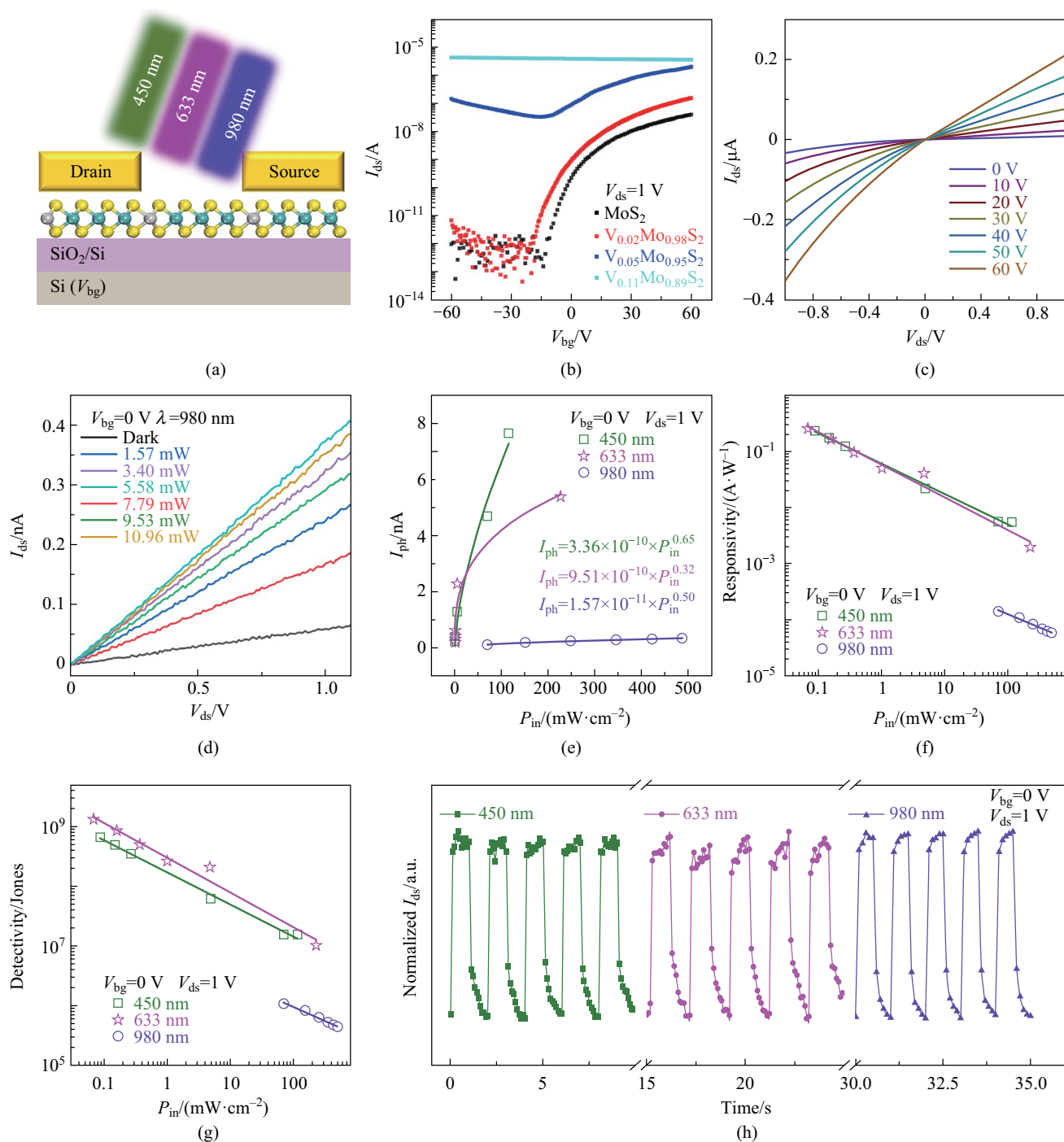


Fig. 5 Electrical transport and photoelectric properties of V-doped MoS₂ monolayers. **a** Device schematic diagram of V-doped MoS₂. **b** Transfer characteristics of the MoS₂, V_{0.02}Mo_{0.98}S₂, V_{0.05}Mo_{0.95}S₂ and V_{0.11}Mo_{0.89}S₂ monolayers, showing the transfer behavior from n- to ambipolar to p-type, respectively. **c** Output characteristics of the V_{0.02}Mo_{0.98}S₂ transistor. **d** $I_{ds} - V_{ds}$ curves of the V-doped MoS₂ device measured in dark and under illumination by 980 nm laser with different incident power densities. **e** Photocurrent, **f** responsivity and **g** detectivity as a function of illumination power density under illumination by 450, 633 and 980 nm lasers, respectively. **h** Time-resolved photoresponse of the V-doped MoS₂ device under illumination by 450, 633 and 980 nm lasers

Table 3 Performances of the V-doped MoS₂ photodetectors under different laser illumination

Laser wavelength/nm	Responsivity at 1 V (A·W ⁻¹)	Detectivity/Jones
450	0.23	6.59 × 10 ⁸
633	0.25	1.31 × 10 ⁹
980	1.41 × 10 ⁻⁴	1.07 × 10 ⁶

different power densities. It is clear that, the channel current increased gradually with increases in the power densities (P_{in}), which demonstrated that the V-doped MoS₂ monolayer has good visible light response. It is worth noting that our V-doped MoS₂ monolayer device exhibited significant light response under illumination by near infrared light at a wavelength of 980 nm; the $I_{ds}-V_{ds}$ curves are shown in Fig. 5d. The obtained extracted photocurrents ($I_{ph} = I_{light} - I_{dark}$) under illumination by different laser power are shown in Fig. 5e, fitted with an equation of $I_{ph} = aP^\alpha$. The fitted parameter of a were 3.36×10^{-10} , 9.51×10^{-10} and 1.57×10^{-11} ; and α were 0.65, 0.32 and 0.50 under illumination by 450, 633 and 980 nm lasers, respectively. The responsivity (R) was calculated by the equation of $R = I_{ph}/(P \times A)$, where I_{ph} is the photocurrent, P is the incident light power density, and A is the effective area of the device channel ($A = 1207.44 \mu\text{m}^2$). As shown in Fig. 5f, the responsivity of the device based on V-doped MoS₂ monolayer reached up to 0.23, 0.25 and 1.41×10^{-4} A/W under illumination by 450, 633 and 980 nm lasers, respectively. Detectivity (D^*) is used to characterize the sensitivity of a photodetector, which can be estimated by $D^* = RA^{1/2}/(2e \times I_{dark})^{1/2}$. The maximum estimated D^* values were 6.59×10^8 , 1.31×10^9 and 1.07×10^6 Jones under illumination by 450, 633 and 980 nm lasers, respectively (Fig. 5g). The summarized result of the responsivity and detectivity is shown in Table 3. The performance comparison between the photodetectors based on V-doped MoS₂ monolayer and other reported photodetectors is shown in Table S1, which demonstrates that our photodetectors have moderate performance [44–52]. Figure 5h shows the switching behavior of the photodetector measured under light irradiation with visible light 450 (green line), 633 (red line) and near-infrared light 980 nm (violet line) lasers, indicating that the device could be switched effectively between high resistance and low resistance states. As shown in Fig. S3, in V-doped MoS₂ monolayers, an accept band lever caused by V doping between the conduction band and valence band can be introduced, which can facilitate the absorption of short-wavelength light, enabling near-infrared light detection. The above results indicate that the V-doped MoS₂ device exhibits significant broad spectral response.

4 Conclusion

In summary, a series of substitutional V-doped MoS₂ monolayers were synthesized using an alkali metal-assisted CVD growth method. The samples were systematically characterized by XPS, Raman, STEM and electrical transport characterizations, confirming that V atoms were uniformly doped into the MoS₂ samples. Interestingly, enhanced B-exciton emission was observed in the doped samples and the emission behaviors were systematically studied using steady temperature-dependent PL experiments. Electrical transport measurements indicated that enhanced p-type conduction occurred in the achieved V-doped MoS₂ monolayers. Moreover, the photodetector based on V-doped MoS₂ monolayer showed broad spectral response from visible to near-infrared light. The synthesized V-doped MoS₂ nanosheets can provide new material platform for spintronics related fundamental research and device applications.

Supplementary Information The online version contains supplementary material available at <https://doi.org/10.1007/s12200-023-00097-w>.

Acknowledgements This research was supported by the National Key R&D Program of China (No. 2022YFA1204300); the National Natural Science Foundation of China (Grant Nos. 62104066, 52372146, U22A20138, 52221001 and 62090035); the Open Project Program of Wuhan National Laboratory for Optoelectronics (No. 2020WNLOKF016); the Science and Technology Innovation Program of Hunan Province (Nos. 2021RC3061 and 2020RC2028); and the National Postdoctoral Program for Innovative Talents (No. BX2021094).

Author contributions BZ, DL and SL designed and performed experiments, and wrote the manuscript. XS and CZ advised on devices measurements. WZ advised on optical measurements. MC advised on STEM measurements. BZ advised on AFM measurements. AP, DL and SL advised on analyzing the results, and provided theoretical guidance. All authors discussed results, commented on them, and edited.

Availability of data and materials The data that support the findings of this study are available from the corresponding author, upon reasonable request.

Declarations

Competing interests The authors declare that they have no competing interests.

Open Access This article is licensed under a Creative Commons Attribution 4.0 International License, which permits use, sharing, adaptation, distribution and reproduction in any medium or format, as long as you give appropriate credit to the original author(s) and the source, provide a link to the Creative Commons licence, and indicate if changes were made. The images or other third party material in this article are included in the article's Creative Commons licence, unless indicated otherwise in a credit line to the material. If material is not included in the article's Creative Commons licence and your intended use is not permitted by statutory regulation or exceeds the permitted use, you will need to obtain permission directly from the copyright holder. To view a copy of this licence, visit <http://creativecommons.org/licenses/by/4.0/>.

References

- Li, W., Gong, X., Yu, Z., Ma, L., Sun, W., Gao, S., Koroglu, C., Wang, W., Liu, L., Li, T., Ning, H., Fan, D., Xu, Y., Tu, X., Xu, T., Sun, L., Wang, W., Lu, J., Ni, Z., Li, J., Duan, X., Wang, P., Nie, Y., Qiu, H., Shi, Y., Pop, E., Wang, J., Wang, X.: Approaching the quantum limit in two-dimensional semiconductor contacts. *Nature* **613**(7943), 274–279 (2023)
- Kang, K., Xie, S., Huang, L., Han, Y., Huang, P.Y., Mak, K.F., Kim, C.-J., Muller, D., Park, J.: High-mobility three-atom-thick semiconducting films with wafer-scale homogeneity. *Nature* **520**(7549), 656–660 (2015)
- Radisavljevic, B., Radenovic, A., Brivio, J., Giacometti, V., Kis, A.: Single-layer MoS₂ transistors. *Nat. Nanotech.* **6**(3), 147–150 (2011)
- Zi, Y., Zhu, J., Hu, L., Wang, M., Huang, W.: Nanoengineering of tin monosulfide (SnS)-based structures for emerging applications. *Small Science* **2**(3), 2100098 (2022)
- Li, T., Guo, W., Ma, L., Li, W., Yu, Z., Han, Z., Gao, S., Liu, L., Fan, D., Wang, Z., Yang, Y., Lin, W., Luo, Z., Chen, X., Dai, N., Tu, X., Pan, D., Yao, Y., Wang, P., Nie, Y., Wang, J., Shi, Y., Wang, X.: Epitaxial growth of wafer-scale molybdenum disulfide semiconductor single crystals on sapphire. *Nat. Nanotech.* **16**(11), 1201–1207 (2021)
- Lin, Z., Liu, Y., Halim, U., Ding, M., Liu, Y., Wang, Y., Jia, C., Chen, P., Duan, X., Wang, C., Song, F., Li, M., Wan, C., Huang, Y., Duan, X.: Solution-processable 2D semiconductors for high-performance large-area electronics. *Nature* **562**(7726), 254–258 (2018)
- Huang, W., Zhu, J., Wang, M., Hu, L., Tang, Y., Shu, Y., Xie, Z., Zhang, H.: Emerging mono-elemental bismuth nanostructures: controlled synthesis and their versatile applications. *Adv. Funct. Mater. Funct. Mater.* **31**(10), 2007584 (2021)
- Lopez-Sanchez, O., Lembke, D., Kayci, M., Radenovic, A., Kis, A.: Ultrasensitive photodetectors based on monolayer MoS₂. *Nat. Nanotech.* **8**(7), 497–501 (2013)
- Zhu, J., Wei, S., Tang, J., Hu, Y., Dai, X., Zi, Y., Wang, M., Xiang, Y., Huang, W.: MXene V₂CTx nanosheet/bismuth quantum dot-based heterostructures for enhanced flexible photodetection and nonlinear photonics. *ACS Appl. Nano Mater.* **6**(14), 13629–13636 (2023)
- Huang, W., Wang, M., Hu, L., Wang, C., Xie, Z., Zhang, H.: Recent advances in semiconducting mono-elemental selenium nanostructures for device applications. *Adv. Funct. Mater. Funct. Mater.* **30**(42), 2003301 (2020)
- Wang, C., Xu, J., Wang, Y., Song, Y., Guo, J., Huang, W., Ge, Y., Hu, L., Liu, J., Zhang, H.: MXene (Ti₂NTx): synthesis, characteristics and application as a thermo-optical switcher for all-optical wavelength tuning laser. *Sci. China Mater.* **64**(1), 259–265 (2021)
- Rong, K., Duan, X., Wang, B., Reichenberg, D., Cohen, A., Liu, C.-L., Mohapatra, P.K., Patsha, A., Gorovoy, V., Mukherjee, S., Kleiner, V., Ismach, A., Koren, E., Hasman, E.: Spin-valley Rashba monolayer laser. *Nat. Mater.* **22**(9), 1085–1093 (2023)
- Zi, Y., Hu, Y., Pu, J., Wang, M., Huang, W.: Recent progress in interface engineering of nanostructures for photoelectrochemical energy harvesting applications. *Small* **19**(19), 2208274 (2023)
- Mak, K.F., He, K., Shan, J., Heinz, T.F.: Control of valley polarization in monolayer MoS₂ by optical helicity. *Nat. Nanotech.* **7**(8), 494 (2012)
- Huang, W., Ma, C., Li, C., Zhang, Y., Hu, L., Chen, T., Tang, Y., Ju, J., Zhang, H.: Highly stable MXene (V₂CTx)-based harmonic pulse generation. *Nanophotonics* **9**(8), 2577–2585 (2020)
- Mak, K.F., Lee, C., Hone, J., Shan, J., Heinz, T.F.: Atomically thin MoS₂: a new direct-gap semiconductor. *Phys. Rev. Lett.* **105**(13), 136805 (2010)
- Steinhoff, A., Kim, J.H., Jahnke, F., Rosner, M., Kim, D.S., Lee, C., Han, G.H., Jeong, M.S., Wehling, T.O., Gies, C.: Efficient excitonic photoluminescence in direct and indirect band gap monolayer MoS₂. *Nano Lett.* **15**(10), 6841–6847 (2015)
- Wu, F., Qu, F., MacDonald, A.H.: Exciton band structure of monolayer MoS₂. *Phys. Rev. B* **91**(7), 075310 (2015)
- Cheiwchanchamnangij, T., Lambrecht, W.R.L.: Quasiparticle band structure calculation of monolayer, bilayer, and bulk MoS₂. *Phys. Rev. B* **85**(20), 205302 (2012)
- Splendiani, A., Sun, L., Zhang, Y., Li, T., Kim, J., Chim, C.-Y., Galli, G., Wang, F.: Emerging photoluminescence in monolayer MoS₂. *Nano Lett.* **10**(4), 1271–1275 (2010)
- Berghäuser, G., Malic, E.: Analytical approach to excitonic properties of MoS₂. *Phys. Rev. B* **89**(12), 125309 (2014)
- Zhou, W., Zou, X., Najmaei, S., Liu, Z., Shi, Y., Kong, J., Lou, J., Ajayan, P.M., Yakobson, B.I., Idrobo, J.-C.: Intrinsic structural defects in monolayer molybdenum disulfide. *Nano Lett.* **13**(6), 2615–2622 (2013)
- Addou, R., Colombo, L., Wallace, R.M.: Surface defects on natural MoS₂. *ACS Appl. Mater. Interfaces* **7**(22), 11921–11929 (2015)
- Duong, D.L., Yun, S.J., Kim, Y., Kim, S.-G., Lee, Y.H.: Long-range ferromagnetic ordering in vanadium-doped WSe₂ semiconductor. *Appl. Phys. Lett.* **115**(24), 242406 (2019)
- Fan, S., Yun, S.J., Yu, W.J., Lee, Y.H.: Tailoring quantum tunneling in a vanadium-doped WSe₂/SnSe₂ heterostructure. *Adv. Sci.* **7**(3), 1902751 (2020)
- Duan, H., Guo, P., Wang, C., Tan, H., Hu, W., Yan, W., Ma, C., Cai, L., Song, L., Zhang, W., Sun, Z., Wang, L., Zhao, W., Yin, Y., Li, X., Wei, S.: Beating the exclusion rule against the coexistence of robust luminescence and ferromagnetism in chalcogenide monolayers. *Nat. Commun.* **10**(1), 1584 (2019)
- Zhou, J., Lin, J., Sims, H., Jiang, C., Cong, C., Brehm, J.A., Zhang, Z., Niu, L., Chen, Y., Zhou, Y., Wang, Y., Liu, F., Zhu, C., Yu, T., Suenaga, K., Mishra, R., Pantelides, S.T., Zhu, Z.-G., Gao, W., Liu, Z., Zhou, W.: Synthesis of co-doped MoS₂ monolayers with enhanced valley splitting. *Adv. Mater.* **32**(29), 2003123 (2020)
- Zou, J., Cai, Z., Lai, Y., Tan, J., Zhang, R., Feng, S., Wang, G., Lin, J., Liu, B., Cheng, H.-M.: Doping concentration modulation in vanadium-doped monolayer molybdenum disulfide for synaptic transistors. *ACS Nano* **15**(4), 7340–7347 (2021)
- Zhang, L., Wang, Z., Zhang, J., Chen, B., Liang, Z., Quan, X., Dai, Y., Huang, J., Wang, Y., Liang, S.-J., Long, M., Si, M., Miao, F., Peng, Y.: Quasi-continuous tuning of carrier polarity in monolayered molybdenum dichalcogenides through substitutional vanadium doping. *Adv. Funct. Mater. Funct. Mater.* **32**(46), 2204760 (2022)
- Zhang, J., Zhu, Y., Tebyetekerwa, M., Li, D., Liu, D., Lei, W., Wang, L., Zhang, Y., Lu, Y.: Vanadium-doped monolayer MoS₂ with tunable optical properties for field-effect transistors. *ACS Appl. Nano Mater.* **4**(1), 769–777 (2020)
- Zhou, J., Lin, J., Huang, X., Zhou, Y., Chen, Y., Xia, J., Wang, H., Xie, Y., Yu, H., Lei, J., Wu, D., Liu, F., Fu, Q., Zeng, Q., Hsu, C.H., Yang, C., Lu, L., Yu, T., Shen, Z., Lin, H., Yakobson, B.I., Liu, Q., Suenaga, K., Liu, G., Liu, Z.: A library of atomically thin metal chalcogenides. *Nature* **556**(7701), 355–359 (2018)
- Li, S., Wang, S., Tang, D.-M., Zhao, W., Xu, H., Chu, L., Bando, Y., Golberg, D., Eda, G.: Halide-assisted atmospheric pressure growth of large WSe₂ and WS₂ monolayer crystals. *Appl. Mater. Today* **1**(1), 60–66 (2015)
- Ganta, D., Sinha, S., Haasch, R.T.: 2-D material molybdenum disulfide analyzed by XPS. *Surf. Sci. Spectra* **21**(1), 19–27 (2014)
- Qin, J.-K., Shao, W.-Z., Xu, C.-Y., Li, Y., Ren, D.-D., Song, X.-G., Zhen, L.: Chemical vapor deposition growth of degenerate p-Type

- Mo-doped ReS₂ films and their homojunction. *ACS Appl. Mater. Interfaces* **9**(18), 15583–15591 (2017)
35. Gao, J., Kim, Y.D., Liang, L., Idrobo, J.C., Chow, P., Tan, J., Li, B., Li, L., Sumpter, B.G., Lu, T.-M., Meunier, V., Hone, J., Koratkar, N.: Transition-metal substitution doping in synthetic atomically thin semiconductors. *Adv. Mater.* **28**(44), 9735–9743 (2016)
 36. Gao, D., Xue, Q., Mao, X., Wang, W., Xu, Q., Xue, D.: Ferromagnetism in ultrathin VS₂ nanosheets. *J. Mater. Chem. C* **1**(37), 5909–5916 (2013)
 37. Li, Y., Zhang, J., Zheng, G., Sun, Y., Hong, S.S., Xiong, F., Wang, S., Lee, H.R., Cui, Y.: Lateral and vertical two-dimensional layered topological insulator heterostructures. *ACS Nano* **9**(11), 10916–10921 (2015)
 38. Fang, W., Zhao, H., Xie, Y., Fang, J., Xu, J., Chen, Z.: Facile hydrothermal synthesis of VS₂/graphene nanocomposites with superior high-rate capability as lithium-ion battery cathodes. *ACS Appl. Mater. Interfaces* **7**(23), 13044–13052 (2015)
 39. Sasaki, S., Kobayashi, Y., Liu, Z., Suenaga, K., Maniwa, Y., Miyauchi, Y., Miyata, Y.: Growth and optical properties of Nb-doped WS₂ monolayers. *Appl. Phys. Express* **9**(7), 071201 (2016)
 40. Ly, T.H., Yun, S.J., Thi, Q.H., Zhao, J.: Edge delamination of monolayer transition metal dichalcogenides. *ACS Nano* **11**(7), 7534–7541 (2017)
 41. Kaplan, D., Mills, K., Lee, J., Torrel, S., Swaminathan, V.: Excitation intensity dependent photoluminescence of annealed two-dimensional MoS₂ grown by chemical vapor deposition. *J. Appl. Phys.* **119**(21), 214301 (2016)
 42. Yan, T., Qiao, X., Liu, X., Tan, P., Zhang, X.: Photoluminescence properties and exciton dynamics in monolayer WSe₂. *Appl. Phys. Lett.* **105**(10), 101901 (2014)
 43. Tiong, K.K., Shou, T.S., Ho, C.H.: Temperature dependence piezoreflectance study of the effect of doping MoS₂ with rhenium. *J. Phys. Condens. Matter* **12**(14), 3441 (2000)
 44. Perea-López, N., Lin, Z., Pradhan, N.R., Iñiguez-Rábago, A., Laura Elías, A., McCreary, A., Lou, J., Ajayan, P.M., Terrones, H., Balicas, L., Terrones, M.: CVD-grown monolayered MoS₂ as an effective photosensor operating at low-voltage. *2D Mater.* **1**(1), 011004 (2014)
 45. Nie, C., Yu, L., Wei, X., Shen, J., Lu, W., Chen, W., Feng, S., Shi, H.: Ultrafast growth of large-area monolayer MoS₂ film via gold foil assistant CVD for a highly sensitive photodetector. *Nanotechnology* **28**(27), (2017)
 46. Zhou, Y.H., An, H.N., Gao, C., Zheng, Z.Q., Wang, B.: UV–Vis–NIR photodetector based on monolayer MoS₂. *Mater. Lett.* **237**, 298–302 (2019)
 47. Zhang, W., Chiu, M.-H., Chen, C.-H., Chen, W., Li, L.-J., Wee, A.T.S.: Role of metal contacts in high-performance phototransistors based on WSe₂ monolayers. *ACS Nano* **8**(8), 8653–8661 (2014)
 48. Sun, M., Fang, Q., Xie, D., Sun, Y., Qian, L., Xu, J., Xiao, P., Teng, C., Li, W., Ren, T., Zhang, Y.: Heterostructured graphene quantum dot/WSe₂/Si photodetector with suppressed dark current and improved detectivity. *Nano Res.* **11**(6), 3233–3243 (2018)
 49. Vabbina, P., Choudhary, N., Chowdhury, A.-A., Sinha, R., Karabiyik, M., Das, S., Choi, W., Pala, N.: Highly sensitive wide bandwidth photodetector based on internal photoemission in CVD grown p-type MoS₂/graphene Schottky Junction. *ACS Appl. Mater. Interfaces* **7**(28), 15206–15213 (2015)
 50. Yang, T., Zheng, B., Wang, Z., Xu, T., Pan, C., Zou, J., Zhang, X., Qi, Z., Liu, H., Feng, Y., Hu, W., Miao, F., Sun, L., Duan, X., Pan, A.: Van der Waals epitaxial growth and optoelectronics of large-scale WSe₂/SnS₂ vertical bilayer p-n junctions. *Nat. Commun.* **8**(1), 1906 (2017)
 51. Zou, Z., Li, D., Liang, J., Zhang, X., Liu, H., Zhu, C., Yang, X., Li, L., Zheng, B., Sun, X., Zeng, Z., Yi, J., Zhuang, X., Wang, X., Pan, A.: Epitaxial synthesis of ultrathin beta-In₂Se₃/MoS₂ heterostructures with high visible/near-infrared photoresponse. *Nanoscale* **12**(11), 6480–6488 (2020)
 52. Sun, X., Liu, Y., Shi, J., Si, C., Du, J., Liu, X., Jiang, C., Yang, S.: Controllable synthesis of 2H–1T' Mo_xRe_(1-x)S₂ lateral heterostructures and their tunable optoelectronic properties. *Adv. Mater.* **35**(38), 2304171 (2023)



Biyuan Zheng is a Postdoctoral Fellow in the College of Materials Science and Engineering, Hunan University, China. He received his B.Sc. degree in the School of Chemistry and Chemical Engineering in 2014, and his Ph.D. degree in the School of Physics and Electronics in 2020 from Hunan University. His research interests mainly focus on synthesis of novel 2D semiconductor nanostructures for optical and electrical applications.



Xingxia Sun received her Ph.D. degree in the College of Materials Science and Engineering in 2022 from Hunan University, China. She is now a Postdoctoral Fellow at the College of Materials Science and Engineering, Hunan University. Her main research interests include the synthesis of nanomaterials with controlled CVD route, and their applications in photoelectric devices.



Weihao Zheng is an associate professor in National University of Defense Technology (NUDT), China. He received his Ph.D. degree from the School of Physics and Electronics, Hunan University, China in 2019. Afterwards, he worked as an associate researcher at the College of Materials Science and Engineering, Hunan University (2019–2022). His research interests focus on the carrier dynamics in 2D semiconductor heterostructures and the fabrication of the multi-functional lasers based on the nanomaterials.



Chenguang Zhu received his Ph.D. degree in the College of Materials Science and Engineering in 2022 from Hunan University, China. He is now a Postdoctoral Fellow at the College of Materials Science and Engineering, Hunan University. His research interests mainly include the fabrication of nanodevices, the performance and application of kinds of semiconductor materials.



Dong Li received his B.Sc. degree in 2013 and Ph.D. degrees in 2018 from the School of Physical Science and Engineering, Tongji University, China. Afterwards, he joined the Key Laboratory for Micro Nano Physics and Technology of Hunan Province in Hunan University, China as a professor. His research interests include low-dimensional materials, devices and their applications in future electronics and optoelectronics.



Chao Ma is a professor in the College of Materials Science and Engineering, Hunan University, China. He received his B.Sc. degree from the School of Physics and Technology, Wuhan University, China in 2004. He received his Ph.D. degree from the Institute of Physics, Chinese Academy of Sciences, China in 2009. Afterwards, he worked as a visiting scholar at Brookhaven National Laboratory, USA (2009–2011), and as an assistant research fellow (2009–2012), and as an associate

research fellow (2012–2014) at the Institute of Physics, Chinese Academy of Sciences, and as an associate professor at University of Science and Technology of China (2014–2017). His current research interests focus on the transmission electron microscopy study of functional materials, including transition metal oxide heterojunctions, multiferroic materials and new energy materials.



Shengman Li received her B.Sc. degree in 2015 and Ph.D. degree in 2020 in the School of Optics and Electronic Information, Huazhong University of Science and Technology (HUST), China. Afterwards, she joined the College of Materials Science and Engineering, Hunan University, China as an associate professor (2020.07–2022.01). Her research interests mainly focus on low-dimensional materials, devices and their applications in future electronics and optoelectronics.



Anlian Pan received his Ph.D. degree from the Institute of Physics, Chinese Academy of Sciences, China in 2006. Afterwards, he worked for one year as a Humboldt Research Fellow with Prof. Ulrich Goesele at Max Planck Institute of Microstructure Physics, Germany, and then joined Arizona State University, USA as a Postdoctoral Fellow, where he became a research assistant professor. He came back to Hunan University, China in 2010 and has been working as the distinguished professor of

“Furong” scholar in Hunan Province since then. His research interests include the micro-nano optical, electronics of semiconductor nanostructures.